





# Microstructural white matter integrity in relation to vascular reactivity in Dutch-type hereditary cerebral amyloid angiopathy

Journal of Cerebral Blood Flow & Metabolism  
2023, Vol. 43(12) 2144–2155  
© The Author(s) 2023



Article reuse guidelines:  
sagepub.com/journals-permissions  
DOI: 10.1177/0271678X231200425  
journals.sagepub.com/home/jcbfm



Manon R Schipper<sup>1,\*</sup> , Naomi Vlegels<sup>2,3,\*</sup>,  
Thijs W van Harten<sup>1</sup> , Ingeborg Rasing<sup>4</sup>, Emma A Koemans<sup>4</sup>,  
Sabine Voigt<sup>1,4</sup>, Alberto de Luca<sup>2,5</sup>, Kanishk Kaushik<sup>4</sup> ,  
Ellis S van Etten<sup>4</sup>, Erik W van Zwet<sup>6</sup>, Gisela M Terwindt<sup>4</sup>,  
Geert Jan Biessels<sup>2</sup>, Matthias JP van Osch<sup>1</sup> ,  
Marianne AA van Walderveen<sup>1</sup> and Marieke JH Wermer<sup>4,7</sup>

## Abstract

Cerebral Amyloid Angiopathy (CAA) is characterized by cerebrovascular amyloid- $\beta$  accumulation leading to hallmark cortical MRI markers, such as vascular reactivity, but white matter is also affected. By studying the relationship in different disease stages of Dutch-type CAA (D-CAA), we tested the relation between vascular reactivity and microstructural white matter integrity loss. In a cross-sectional study in D-CAA, 3 T MRI was performed with Blood-Oxygen-Level-Dependent (BOLD) fMRI upon visual activation to assess vascular reactivity and diffusion tensor imaging to assess microstructural white matter integrity through Peak Width of Skeletonized Mean Diffusivity (PSMD). We assessed the relationship between BOLD parameters – amplitude, time-to-peak (TTP), and time-to-baseline (TTB) – and PSMD, with linear and quadratic regression modeling. In total, 25 participants were included (15/10 pre-symptomatic/symptomatic; mean age 36/59 y). A lowered BOLD amplitude (unstandardized  $\beta = 0.64$ , 95%CI [0.10, 1.18],  $p = 0.02$ , Adjusted  $R^2 = 0.48$ ), was quadratically associated with increased PSMD levels. A delayed BOLD response, with prolonged TTP ( $\beta = 8.34 \times 10^{-6}$ , 95%CI [ $1.84 \times 10^{-6}$ ,  $1.48 \times 10^{-5}$ ],  $p = 0.02$ , Adj.  $R^2 = 0.25$ ) and TTB ( $\beta = 6.57 \times 10^{-6}$ , 95%CI [ $1.92 \times 10^{-6}$ ,  $1.12 \times 10^{-5}$ ],  $p = 0.008$ , Adj.  $R^2 = 0.29$ ), was linearly associated with increased PSMD. In D-CAA subjects, predominantly in the symptomatic stage, impaired cerebrovascular reactivity is related to microstructural white matter integrity loss. Future longitudinal studies are needed to investigate whether this relation is causal.

## Keywords

Diffusion magnetic resonance imaging, vascular reactivity, functional magnetic resonance imaging, cerebral amyloid angiopathy, Dutch-type hereditary cerebral amyloid angiopathy

Received 4 May 2023; Revised 4 August 2023; Accepted 7 August 2023

<sup>1</sup>Department of Radiology, Leiden University Medical Center, Leiden, The Netherlands

<sup>2</sup>Department of Neurology and Neurosurgery, UMC Utrecht Brain Center, University Medical Center Utrecht, Utrecht, The Netherlands

<sup>3</sup>Institute for Stroke and Dementia Research, University Hospital, LMU Munich, Munich, Germany

<sup>4</sup>Department of Neurology, Leiden University Medical Center, Leiden, The Netherlands

<sup>5</sup>Image Sciences Institute, University Medical Center Utrecht, Utrecht University, Utrecht, The Netherlands

<sup>6</sup>Department of Biostatistics, Leiden University Medical Center, Leiden, The Netherlands

<sup>7</sup>Department of Neurology, University Medical Center Groningen, Groningen, The Netherlands

\*These authors contributed equally to this work.

## Corresponding author:

Manon R Schipper, Leiden University Medical Center, Albinusdreef 2, 2300 RC Leiden, The Netherlands.  
Email: m.r.schipper@lumc.nl

## Introduction

Cerebral Amyloid Angiopathy (CAA) is one of the leading etiologies of lobar intracerebral hemorrhage (ICH) and cognitive decline in elderly.<sup>1</sup> CAA is characterized by amyloid- $\beta$  (A $\beta$ ) deposition in the cortical and leptomeningeal vasculature of the brain.<sup>2</sup> This deposition may cause vessel rigidity, and limit smooth muscle cell functioning, making the affected vessels more prone to rupture. On MRI, markers that are associated with CAA are – in addition to ICH – lobar cerebral microbleeds (CMB), cortical superficial siderosis (cSS),<sup>3</sup> white matter hyperintensities (WMH), lobar lacunes, cortical microinfarcts (CMI),<sup>4</sup> and enlarged perivascular spaces in the centrum semiovale (CSO-PVS).<sup>5</sup> Hemorrhagic markers and CMIs occur in the cortical region of the brain and colocalize with A $\beta$  accumulation, while other markers – WMH and enlarged PVS – localize in the white matter. This may point towards a remote effect of cortical A $\beta$  accumulation on white matter integrity. Such a remote effect has recently been observed in ex vivo brains, with enlarged PVS in the subcortical white matter being related to A $\beta$  accumulation within the overlying cortical part of the vessel.<sup>6</sup> The mechanisms that underlie these remote effects are still poorly understood.

Quantitative MR techniques provide opportunities to assess alterations in brain tissue that are not visible on conventional MRI.<sup>7</sup> Research in patients with sporadic CAA has shown changes in vascular reactivity of cortical vessels in the occipital lobe, with a lower response amplitude and delayed time-to-peak (TTP) and time-to-baseline (TTB) of the Blood-Oxygen-Level-Dependent (BOLD) measure of visually stimulated functional MRI (fMRI).<sup>7</sup> This impaired vascular reactivity is thought to reflect arterial stiffening, as a consequence of the A $\beta$  deposition within the vessel wall. This hypothesis is strengthened by the comparison of visually evoked potentials and visually stimulated fMRI that has shown that the reduced vascular reactivity is due to impaired functioning of the blood vessels rather than to impaired neuronal firing and accompanying change in metabolic demand.<sup>8</sup> However, it is not completely understood how these hemodynamic changes relate to the widespread white matter integrity loss characteristically observed in CAA. Diffusion MRI is currently the most sensitive measure for white matter integrity in cerebral small vessel disease (cSVD).<sup>9</sup> Previous research has shown altered diffusion measures in CAA, typically with a global increase in mean diffusivity and decrease in directionality of diffusion.<sup>10–12</sup> These altered diffusion measures may indicate microstructural white matter integrity loss in the form of white matter tissue rarefaction and demyelination.<sup>13</sup>

Most cases of CAA are sporadic, but worldwide a few rare autosomal dominant forms exist. One of the most common hereditary forms is Dutch-type hereditary CAA (D-CAA). D-CAA is caused by a single based point mutation at codon 693 of the amyloid precursor protein (APP) gene located on chromosome 21.<sup>14</sup> D-CAA is biochemically, pathologically, and radiologically similar to CAA, but has an earlier time of onset and more aggressive disease course.<sup>15</sup> Genetic testing and the early onset allow us to study CAA pathology with limited influence of age-related confounders, in early as well as progressed disease stages. Measures of vascular reactivity and microstructural white matter integrity have both shown to be affected already in pre-symptomatic D-CAA, in the form of a delayed and lowered vascular response and increased “*Peak Width of Skeletonized Mean Diffusivity*” (PSMD), as measured with Diffusion Tensor Imaging (DTI).<sup>16,17</sup>

We examined the association between BOLD parameters – amplitude, TTP, and TTB – and PSMD in both pre-symptomatic and symptomatic D-CAA mutation carriers to better understand the relationship between hemodynamic alterations in the cortex and loss of microstructural white matter integrity.

## Methods and materials

### Study population

We included pre-symptomatic and symptomatic D-CAA mutation carriers who participated in our ongoing prospective natural history study in D-CAA (AURORA) between February 2018 and July 2021. All participants were recruited via the (outpatient) clinic of the Leiden University Medical Center (LUMC). Inclusion criteria were age  $\geq 18$  years and a DNA proven APP mutation, or a medical history of  $\geq 1$  lobar ICH and  $\geq 1$  first-degree relative with D-CAA. Symptomatic D-CAA was defined by a history of at least one symptomatic ICH. During their study visit, participants underwent an interview (demographics and medical history), blood withdrawal, neuropsychological testing, and a 3 Tesla (T) and 7 T brain MRI scan. To be eligible for this current study, participants needed to have a complete 3 T DTI and fMRI scan of the brain.

This study was in accordance with the Helsinki protocol and approved by the Medical Ethics Committee Leiden The Hague Delft and written informed consent was obtained from all participants before enrollment.

### MRI data acquisition

MRI scans of all D-CAA participants were acquired on a whole-body 3 T magnetic resonance system

(Philips Achieva, Best, the Netherlands) with a standard 32-channel head coil. Three-dimensional T1 weighted images were acquired with the following parameters: repetition time (TR)/echo time (TE) 9.7/4.6 ms, flip angle 7 degrees, 130 slices with no interslice gap, and a field of view (FOV) of  $217 \times 172 \times 156$  mm with a voxel size of  $1.2 \times 1.2 \times 1.2$  mm, resulting in a scan duration of 2:48 min. The visually stimulated BOLD fMRI sequence was acquired using the following parameters: TR/TE 1500/38 ms, flip angle 78 degrees, 18 slices with a 0.5 mm interslice gap, FOV of  $210 \times 177 \times 59$  mm with a voxel size of  $2.50 \times 2.50 \times 2.81$  mm, and 224 dynamics (220 dynamics in 4 participants) resulting in a scan duration of ~5:40 min. The paradigm of the visual stimulus consisted of 7 blocks of an 8 Hz flashing radial black and white checkerboard pattern, for 20 s, followed by a grey screen for 28 s.<sup>7</sup> DTI images were acquired using the following parameters: TR/TE 8194/76 ms, voxel size  $1.72 \times 1.72 \times 2.50$  mm, flip angle 90 degrees, 48 slices with no interslice gap, and FOV of  $220 \times 220 \times 120$  mm, we acquired 45 gradient directions with b-value  $1200 \text{ s/mm}^2$  and one baseline image with b-value  $0 \text{ s/mm}^2$ , resulting in a scan duration 6:33 min. The complete MRI protocol can be found in Supplementary Table 1.

### **BOLD processing**

fMRI data processing was carried out using FEAT (fMRI Expert Analysis Tool)<sup>18</sup> v6.0, part of FSL (FMRIB's Software Library, [www.fmrib.ox.ac.uk/fsl](http://www.fmrib.ox.ac.uk/fsl)). The following pre-statistics processing steps were applied; motion correction using MCFLIRT;<sup>19</sup> slice-timing correction using Fourier-space time-series phase-shifting; non-brain removal using BET;<sup>20</sup> spatial smoothing using a Gaussian kernel of FWHM 3.0 mm; grand-mean intensity normalization of the entire 4D dataset by a single multiplicative factor; highpass temporal filtering (Gaussian-weighted least-squares straight line fitting, with  $\sigma = 24.0$  s). ICA-based exploratory data analysis was carried out using MELODIC,<sup>21</sup> in order to investigate the possible presence of unexpected artefacts or activation. Motion parameters as estimated by MCFLIRT were included as confound explanatory variable in the model, to remove residual effects of motion.

The pre-processed fMRI data were analyzed within the primary visual cortex (V1).<sup>22</sup> Registration of V1 to the fMRI image was performed using FSL FLIRT<sup>19</sup> and FNIRT.<sup>23,24</sup> In patients with one or more ICH, we masked out the voxels in the V1 mask that were affected by ICH and surrounding gliosis, resulting in our region of interest (ROI). ICH and gliosis masks were manually delineated on T1 weighted images by two observers

(MRS and NV) under supervision of an experienced neuroradiologist (MAAvW). The appearance on Fluid-Attenuated Inversion Recovery, susceptibility weighted, and T2 weighted sequences was taken into account while delineating ICH and gliosis masks.

The mean BOLD response in the ROI, per paradigm block, was calculated for each participant. Subsequently, the mean BOLD response was calculated over the 7 paradigm blocks, to filter out noise. A trapezoid fit was applied onto the averaged BOLD response per participant, to determine amplitude, TTP, and TTB of the BOLD response. Calculation of the BOLD parameters was performed in MATLAB R2020b.<sup>25</sup> Amplitude is the percentage signal change of the BOLD response, during the peak of the response, normalized to the baseline. TTP is the amount of time in seconds, from the start of stimulus presentation to the peak of the BOLD response according to the trapezoid fit. TTB is the amount of time in seconds, from the end of stimulus presentation to the return of the BOLD response to baseline. If the BOLD response was too minimal for a trapezoid fit to be applied, the timing parameters were not included for further analysis. Amplitude of the BOLD response was in these cases calculated by taking the maximum of the BOLD response (after excluding outliers that were more than 3 median absolute deviations from the median) and subtracting the baseline BOLD response.

### **Diffusion processing**

DTI data were visually inspected to exclude major artefacts and then the raw diffusion images were pre-processed using the MRtrix v3.0 package<sup>26</sup> (<http://mrtrix.org>) and FSL v6.0.5.<sup>24</sup> Noise and Gibbs ringing artefacts were removed ('dwdennoise', 'mrdegibbs'; MRtrix)<sup>27</sup> and participant motion and eddy current induced distortions were corrected ('eddy'; FSL). Following pre-processing we calculated PSMD v1.8.2 using the fully automated script (<http://www.psm-marker.com>).<sup>28</sup> PSMD is a measure of the dispersion of mean diffusivity (MD) values across the white matter skeleton. To calculate PSMD, diffusion data of each participant was first skeletonized using Tract-Based Spatial Statistics procedure (TBSS),<sup>29</sup> part of FSL, using the FMRIB 1 mm fractional anisotropy (FA) template, thresholded at an FA-value of 0.2. MD images of that same participant were then projected onto the skeleton. To avoid contamination through cerebrospinal fluid partial volume effects, the MD-skeletons were further masked with the template skeleton thresholded at an FA value of 0.3 and a custom mask (provided with PSMD script), designed to exclude regions close to the ventricles. Finally, histogram analysis was performed on this masked MD-skeleton and PSMD was calculated as the

difference between the 95th and 5th percentile of the MD values within the skeleton.

For patients with an ICH, we masked out voxels in the skeleton that were affected by ICH and surrounding gliosis using the earlier described manually delineated masks. The T1 weighted image was registered to diffusion space using FLIRT<sup>19</sup> (part of FSL) and the resulting transformation matrix was applied to the ICH and surrounding gliosis masks. These masks were then provided as lesion mask into the PSMD calculation.

### CAA SVD score

CAA related cSVD score was calculated for each participant.<sup>30</sup> The CAA SVD score consisted of lobar CMBs (1 point for 2–4, 2 points for  $\geq 5$ ), cSS (1 point for focal, 2 points for disseminated), CSO-PVS (1 point for  $\geq 20$ , in one hemisphere and analyzed on one slice), and WMHs (1 point for Fazekas  $\geq 2$ ), resulting in a total CAA cSVD score ranging from 0–6 points, where higher scores reflect a more severe disease burden. The CAA cSVD scores and elaborate description of the scoring of the MRI markers that compose the CAA cSVD score are reported in Supplementary Table 2 and Supplementary Text 1, respectively.

### Statistical analysis

Normality of all variables was assessed with Shapiro-Wilk tests. To correct PSMD for healthy aging, we used the 1000BRAINS cohort for reference.<sup>31,32</sup> Correction was carried out by subtracting age-matched healthy PSMD values from the values in our participants. All analyses described in the results section are performed with the healthy age corrected PSMD data. Results of the analyses with uncorrected PSMD data are presented in Supplementary Text 2, Supplementary Table 3, and Supplementary Figure 1.

To examine the association between vascular reactivity parameters and diffusion MRI measures in pre-symptomatic and symptomatic D-CAA mutation carriers, linear regression analyses were performed with PSMD as dependent variable and BOLD amplitude, TTP, and TTB as independent variables. Addition of quadratic components to the regression analyses were examined by t-tests comparing the linear regression analyses and regression models with the added quadratic components. For each regression analysis, the unstandardized  $\beta$  is reported. A table containing both the standardized and unstandardized  $\beta$  per analysis is presented in Supplementary Table 3. To validate whether the relationship between the PSMD and BOLD would be stronger near the location where the vascular reactivity is measured, we performed an ROI based analysis of the PSMD in the occipital lobe and

plotted the posterior PSMD as a function of age (Supplementary Figure 2) and in relation to the BOLD measures (Supplementary Figure 3). Sensitivity analyses were performed to see if the effects seen in the total group of D-CAA mutation carriers are consistent in the pre-symptomatic D-CAA mutation carriers. No sensitivity analyses were performed for the symptomatic D-CAA mutation carriers due to the small sample of this subgroup.

All statistical analyses were performed using the software R v4.1.0.<sup>33</sup>

## Result

Out of 38 participants who had complete DTI and fMRI scans, 12 participants (five/seven pre-/symptomatic) were excluded due to paradigm related motion (Pearson's  $R > 0.2$ <sup>34</sup>) and one participant was excluded due to failed registration. Thus, we included 25 participants: 15 pre-symptomatic and 10 symptomatic mutation carriers. Five out of 10 symptomatic mutation carriers had a minimal response to the visual stimulus. Therefore, the timing parameters of the fMRI reactivity scans could not be determined in these cases, and only the amplitude parameter was included in the analyses. Characteristics of the participants are presented in Table 1.

### PSMD, BOLD parameters, and age

The uncorrected PSMD in the current D-CAA study cohort, PSMD in the 1000BRAINS cohort, and the healthy age corrected PSMD as a function of age, are depicted in Figure 1. Figure 1 shows that the normal age-effect on PSMD is smaller than the increase in PSMD as observed in our cohort, i.e. disease duration is more dominantly influencing PSMD. BOLD parameters as a function of age in the current D-CAA study cohort, are depicted in Figure 2.

### Healthy age corrected PSMD in relation to BOLD parameters

First, linear regression modeling showed that decreasing amplitude significantly predicted increasing healthy age corrected PSMD (unstandardized  $B = -0.90 \times 10^{-4} \text{ mm}^2/\text{s}/\text{percentage}$ , 95% CI  $[-1.39 \times 10^{-4}, -0.42 \times 10^{-4}]$ ,  $p < 0.001$ , Adjusted  $R^2 = 0.36$ ). Second, linear regression modeling showed that increasing BOLD TTP significantly predicted increasing healthy age corrected PSMD (unstandardized  $B = 8.34 \times 10^{-6} \text{ mm}^2/\text{s}/\text{s}$ , 95% CI  $[1.84 \times 10^{-6}, 1.48 \times 10^{-5}]$ ,  $p = 0.02$ , Adj.  $R^2 = 0.25$ ). Last, linear regression modeling showed that increasing BOLD TTB significantly predicted increasing healthy age corrected PSMD

**Table 1.** Descriptive statistics of the current study cohort.

	Study cohort (n = 25)	Pre-symptomatic mutation carriers (n = 15)	Symptomatic mutation carriers (n = 10)
Mean age $\pm$ SD [y] (range)	45 $\pm$ 13 (28–71)	36 $\pm$ 6 (28–47)	59 $\pm$ 7 (49–71)
Sex (M/F)	9/16	4/11	5/5
Median uncorrected PSMD [ $10^{-4}$ mm <sup>2</sup> /s] (IQR)	3.20 (2.40–4.60)	2.40 (2.30–2.79)	4.70 (4.45–5.43)
Median healthy age corrected PSMD [ $10^{-4}$ mm <sup>2</sup> /s] (IQR)	0.71 (–0.07–1.93)	0.08 (–0.07–0.47)	2.00 (1.58–2.26)
Mean MD score $\pm$ SD [ $10^{-4}$ mm <sup>2</sup> /s] (range)	7.83 $\pm$ 0.65 (6.79–9.31)	7.40 $\pm$ 0.42 (6.79–8.20)	8.47 $\pm$ 0.49 (7.76–9.31)
Mean FA score $\pm$ SD [mm <sup>2</sup> /s] (range)	0.37 $\pm$ 0.05 (0.27–0.44)	0.40 $\pm$ 0.03 (0.35–0.44)	0.32 $\pm$ 0.04 (0.27–0.39)
Mean amplitude of BOLD response $\pm$ SD [%] (range)	1.04 $\pm$ 0.69 (0.26–2.93)	1.41 $\pm$ 0.64 (0.48–2.93)	0.48 $\pm$ 0.18 (0.26–0.76)
Mean TTP of BOLD response $\pm$ SD [s] (range) <sup>a</sup>	15.93 $\pm$ 6.29 (4.77–28.66)	13.49 $\pm$ 4.57 (4.77–23.08)	23.27 $\pm$ 5.02 (17.43–28.66)
Mean TTB of BOLD response $\pm$ SD [s] (range) <sup>a</sup>	19.40 $\pm$ 8.54 (8.74–37.68)	15.66 $\pm$ 5.21 (8.74–24.53)	30.63 $\pm$ 6.46 (25.19–37.68)
Median total CAA cSVD score (IQR) <sup>b</sup>	1 (1–4)	1 (0–1)	5 (4–5)
0	4	4	0
1	6	6	0
2	1	1	0
3	1	0	1
4	3	0	3
5	5	0	5
6	0	0	0

PSMD: Peak Width of Skeletonized Mean Diffusivity; IQR: interquartile range; MD: mean diffusivity; FA: fractional anisotropy; BOLD: Blood-Oxygen-Level-Dependent; TTP: time-to-peak; TTB: time-to-baseline; CAA: Cerebral Amyloid Angiopathy; cSVD: cerebral Small Vessel Disease.

<sup>a</sup>Five missing values in the study cohort and symptomatic D-CAA mutation carriers.

<sup>b</sup>Five, four, and one missing values in the total study cohort, pre-symptomatic, and symptomatic D-CAA mutation carriers, respectively.

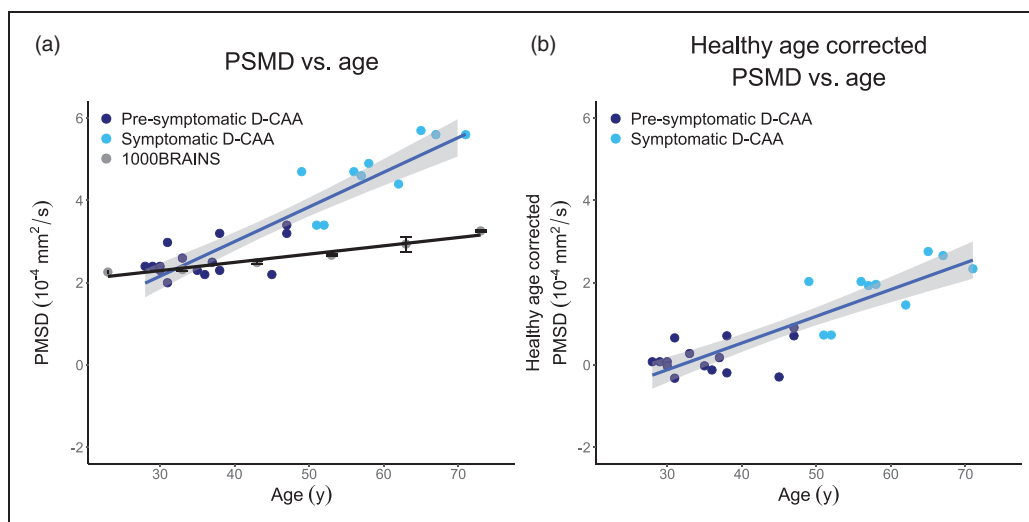


**Figure 1.** (a) uncorrected PSMD as a function of age in the D-CAA study cohort and PSMD in the 1000BRAINS cohort, and (b) healthy age corrected PSMD as a function of age in the D-CAA study cohort. All graphs include linear regression trends. The standard error for the D-CAA dataset is indicated by the shaded error bar and for the 1000BRAINS cohort it is indicated with standard error bars per age group. PSMD: Peak Width Skeletonized Mean Diffusivity; D-CAA; Dutch-type Cerebral Amyloid Angiopathy.

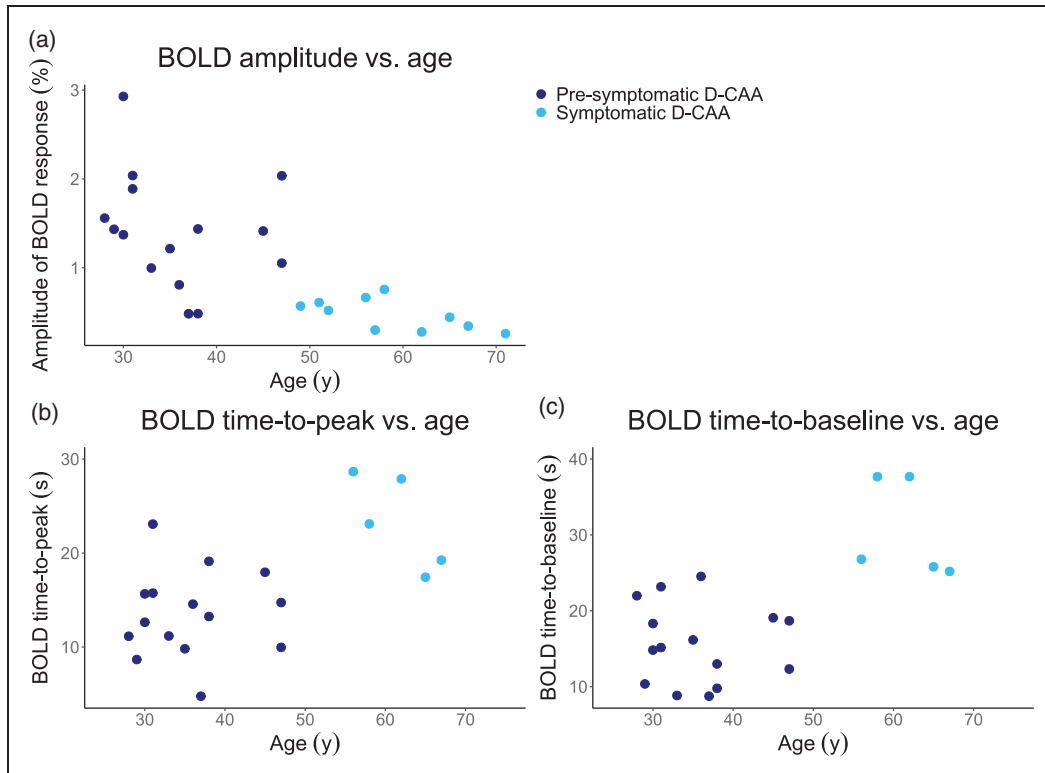


**Figure 2.** BOLD parameters (a) amplitude, (b) time-to-peak, and (c) time-to-baseline as a function of age in the current D-CAA study cohort. BOLD: Blood-Oxygen-Level-Dependent; D-CAA: Dutch-type Cerebral Amyloid Angiopathy.

(unstandardized  $B = 6.57 \times 10^{-6} \text{ mm}^2/\text{s/s}$ , 95% CI  $[1.92 \times 10^{-6}, 1.12 \times 10^{-5}]$ ,  $p = 0.008$ , Adj.  $R^2 = 0.29$ ).

Looking at the relationships between BOLD parameters and healthy age corrected PSMD, a linear fit might not be the best fit. To assess a non-linear relationship, we tested the addition of the independent variables as quadratic components to the regression models. Addition of BOLD amplitude as quadratic effect to the model, led to an increase in explained variance compared to the linear model, while the relation remained statistically significant (unstandardized  $B = 6.38 \times 10^{-5} \text{ mm}^2/\text{s/percentage}$ , 95% CI  $[0.97 \times 10^{-5}, 11.79 \times 10^{-5}]$ ,  $p = 0.02$ , Adj.  $R^2 = 0.48$ ). The quadratic model improved statistically significantly on the linear model ( $p = 0.02$ ). The quadratic regression models with increasing timing parameters – TTP and TTB – as predictors for increasing healthy age corrected PSMD were not significant and are reported in Supplementary Table 3.

Figure 3 shows the linear regressions for healthy age corrected PSMD versus the timing parameters and the quadratic regression between healthy age corrected PSMD versus BOLD amplitude.

**Sensitivity analyses**

Sensitivity analyses in the pre-symptomatic D-CAA mutation carriers showed that the effect size, as

estimated by unstandardized B, collapses in the linear (unstandardized  $B = -0.79 \times 10^{-5} \text{ mm}^2/\text{s/percentage}$ , 95% CI  $[-4.42 \times 10^{-5}, 2.82 \times 10^{-5}]$ ,  $p = 0.64$ , Adj.  $R^2 = -0.06$ ) and quadratic regression modeling (unstandardized  $B = 0.74 \times 10^{-5} \text{ mm}^2/\text{s/percentage}$ , 95% CI  $[-3.63 \times 10^{-5}, 5.12 \times 10^{-5}]$ ,  $p = 0.72$  Adj.  $R^2 = -0.13$ ) of BOLD amplitude as predictor of healthy age corrected PSMD. The sign of the effect size in the linear regression models, as estimated by unstandardized B, turns around for timing parameters TTP (unstandardized  $B = -3.20 \times 10^{-7} \text{ mm}^2/\text{s/s}$ , 95% CI  $[-5.44 \times 10^{-6}, 4.80 \times 10^{-6}]$ ,  $p = 0.90$ , Adj.  $R^2 = -0.08$ ) and TTB (unstandardized  $B = -2.46 \times 10^{-6} \text{ mm}^2/\text{s/percentage}$ , 95% CI  $[-6.71 \times 10^{-6}, 1.80 \times 10^{-6}]$ ,  $p = 0.24$ , Adj.  $R^2 = 0.04$ ) in predicting increasing healthy age corrected PSMD. In addition, these regression models do not show a statistically significant effect.

**Discussion**

The most important findings of this study are two-fold. First, a lowered amplitude of the vascular response is associated with deteriorated microstructural white matter integrity, but only when vascular reactivity is already severely lowered. Second, a delayed vascular

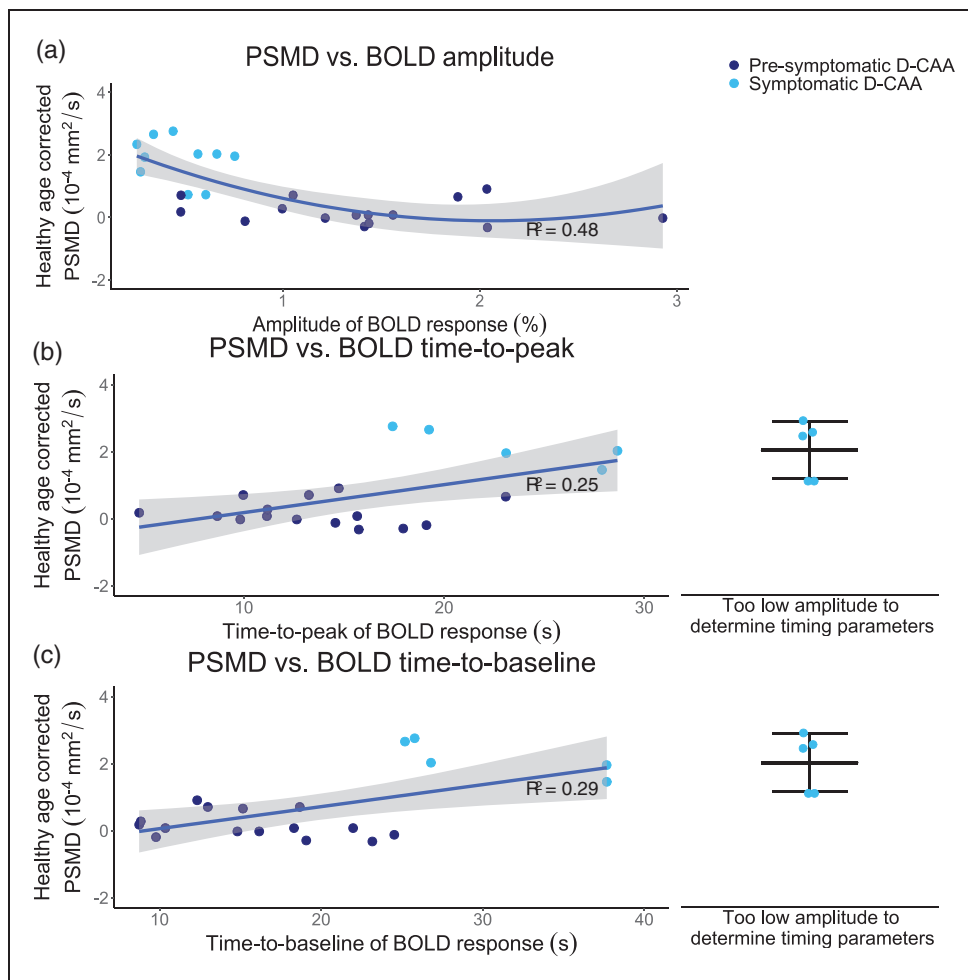


**Figure 3.** Graphs showing the relations between healthy age corrected PSMD and BOLD parameters with corresponding adjusted  $R^2$  values; (a) quadratic relationship between PSMD and BOLD amplitude, (b) linear relationship between PSMD and BOLD time-to-peak, and (c) linear relationship between PSMD and BOLD time-to-baseline. In b and c, the healthy age corrected PSMD values, of symptomatic D-CAA mutation carriers of whom no timing parameter could be calculated due to minimal BOLD response to the visual stimulus, are jittered on the right side of the plot, presenting the mean and standard deviation. PSMD: Peak Width Skeletonized Mean Diffusivity; BOLD: Blood-Oxygen-Level-Dependent; D-CAA: Dutch-type Cerebral Amyloid Angiopathy.

response is also related to deteriorated microstructural white matter integrity.

Sensitivity analyses showed that the effect between the BOLD parameters and PSMD does not hold when solely looking at pre-symptomatic D-CAA mutation carriers. This may be explained by the relatively early disease stage, resulting in a narrow range of values and a concomitant drop in the effect size. Considering the amplitude of the BOLD response, since the amplitude had to decrease significantly before PSMD started to increase, such a correlation might remain undetected in the pre-symptomatic phase. On the other hand, it can also be that our sample size of pre-symptomatic subjects was just too small to replicate the effect found in the total group. No sensitivity analyses were performed in symptomatic D-CAA mutation carriers due to the even smaller subgroup size. This also points to the

general limitation of the current study: the total sample size is limited, which arises from the rarity of the D-CAA genetic variant and due to the exclusion based on stimulus-correlated motion.

Previous literature has shown both lowered vascular reactivity and lowered microstructural white matter integrity in D-CAA with already significant reductions in the pre-symptomatic phase.<sup>16,17</sup> With the current study we increase understanding of potential mechanisms underlying the deterioration in microstructural white matter integrity by studying its association with vascular reactivity. A delayed vascular response to a visual stimulus was found to be linearly – albeit with limited significance – related to increased values of PSMD, and thus lowered microstructural white matter integrity. In contrast, PSMD remained relatively stable along a wide range of amplitude reductions of

the BOLD response. When the vascular reactivity was deteriorated to a degree that only a very small amplitude of the BOLD response (<0.9%) remained, values of PSMD started to increase sharply. Timing parameters of vascular reactivity, therefore, appear to go hand in hand with microstructural white matter integrity loss, while the amplitude of the vascular response only starts to relate to microstructural white matter integrity loss once the vascular response is severely lowered.

The current findings are predominantly affected by the increased PSMD values in the symptomatic D-CAA. In participants with pre-symptomatic D-CAA, there is only a small subgroup with deviating PSMD values compared to the healthy cohort, while the vascular reactivity is already affected in most pre-symptomatic participant. Earlier reduction in vascular reactivity, compared to white matter integrity loss, is in line with the recently proposed pathophysiological framework of CAA.<sup>35</sup> It is therefore likely that part of the participants with pre-symptomatic D-CAA are only in stage two of the disease, that is characterized by amyloid- $\beta$  accumulation and reduced vascular reactivity.<sup>35</sup> The rapid deterioration that we see in the symptomatic stage of D-CAA is thought to be the result of vascular remodeling that accompanies the stage in which mutation carriers get ICH (stage four).<sup>35</sup>

To further interpret our results, we hypothesize that A $\beta$  accumulation in the cortical arteries, arterioles, and capillaries, could be causing vessel rigidity, which first results in a delay and subsequently in a reduction of the vascular response. This increased timing and lowered amplitude of the vascular response may reflect delayed and decreased blood supply not only to the visual cortex, but probably also to the white matter, leading to integrity loss, but only in the more severe stages of disease. A potential reason why integrity loss only occurs for more severe reductions in vascular reactivity may be the relatively low metabolic demand and alternative blood supply of the white matter as well as inherent reserve capacity of cerebral hemodynamics.<sup>36</sup>

The vascular reactivity measurement in the current D-CAA cohort shows a flooring effect for the BOLD timing parameters, where these can no longer be assessed when the vascular response to a visual stimulus is too small. It appeared that five participants had such a lowered vascular response to the visual stimulus, that no trapezoid response could be fitted to the BOLD signal. In these cases, we were only able to estimate the amplitude change of the BOLD response, but no timing parameters could be deducted from the noisy time-courses. Thus, information on the timing parameters of the individuals with the most affected vascular reactivity was excluded from the regression models with timing parameters as predictors. This may have

resulted in an underestimation of the effect between the timing parameters – TTP and TTB – and PSMD.

A limitation to vascular reactivity as measured by visually stimulated fMRI, is that it cannot be ruled out that a so called non-responder did not look at the visual stimulus, and therefore was not visually stimulated. A simple feedback test incorporated into the visual task to check compliance is therefore an important improvement and was previously employed.<sup>7,16</sup> However, during the measurements we did not have any sign of non-compliance from our participants. Another limitation of using a visual stimulus is that the vascular reactivity was only measured in the primary visual cortex. However, previous findings have shown that task-based fMRI assessing the primary visual cortex and the motor cortex have found a moderate correlation to each other and a high correlation with global microbleeds and WMH volume in CAA.<sup>8</sup> Based on these findings, we hypothesize that the measured vascular reactivity is also a reflection of the more global disease effect. However, based on pathological studies, we believe that vascular amyloid- $\beta$  deposition starts especially within the posterior areas of the cerebrum and therefore occipital measures will probably show the earliest reduction in vascular reactivity.<sup>37,38</sup> In addition, 12 participants had to be excluded due to stimulus-correlated motion during the fMRI scan. This may have resulted in an inclusion bias. However, since excluded participants were both pre-symptomatic and symptomatic patients, we do not believe that this e.g. has led to exclusion of the most affected participants. Finally, to further investigate and provide evidence for the relationship between impaired cerebrovascular reactivity and microstructural white matter integrity or study causality, a follow up study is needed.

By excluding lesions from our V1 ROI for the BOLD analysis and PSMD skeleton for the PSMD analysis, we have excluded a direct effect of signal drops due to ICH on our analyses. However, since often times both hemisphere are ICH-affect, it is not feasible to perform a non-ICH hemisphere analysis for PSMD and BOLD. A resulting limitation is that we cannot differentiate between microstructural related CAA and large scale CAA effects. It, therefore, cannot be ruled out that abnormal BOLD reflects Wallerian degeneration caused by ICH.

It is likely that the large variance in the BOLD measures, that is especially present in the pre-symptomatic mutation carriers, contributes to the lack of a significant relationship between PSMD and BOLD in pre-symptomatic mutation carriers. However, the variance in BOLD amplitude as observed in our study is similar to that of healthy controls,<sup>16,39</sup> most likely indicating that this reflects normal biological variation. In symptomatic mutation carriers a much smaller variance was



observed, what can be attributed to a flooring effect of the BOLD amplitude. Previous results did show a lower variance in the timing parameters in healthy controls compared to the subjects in this study, which is likely due to the impact on the effect of pathology on timing parameters in D-CAA. This pathology, and therefore increased variance in the BOLD timing measures, may partly be attributed to the fact that loss of vasoreactivity typically precedes non-hemorrhagic injury,<sup>35</sup> such as reflected by the lower PSMD in older mutation carriers.

Limiting the PSMD measurements to the occipital lobe, as presented in Supplementary Figures 2 and 3, shows that the association remains very similar in comparison to whole brain PSMD. This may indicate either that similar mechanisms are at play in the occipital lobe as whole brain or that the posterior white matter integrity loss drives the whole brain PSMD values.

With the current study we cannot assess if the found relationship is specific for CAA, or whether it is generalizable for other cSVD. However, we think the studied association and measure of vascular reactivity are especially interesting in (D-)CAA as visually stimulated fMRI is most often used to assess vascular reactivity.<sup>7,16,39–43</sup> Vascular reactivity in the occipital cortex is especially interesting since amyloid- $\beta$  accumulation starts predominantly in the posterior cortex.<sup>37,38</sup> In addition, it has been shown that both vascular response and white matter integrity area already affected in the pre-symptomatic phase of (D-)CAA,<sup>16,35</sup> which leads us to believe that the relationship between BOLD and PSMD is of special interest in the pre-symptomatic phase of CAA.

Our study adds to the current knowledge by studying invisible white matter integrity loss, which may already show differences in the earliest phases of the disease course. Therefore, the monogenetic background of our participant population adds importantly to the relevance, as we can study the pre-symptomatic stage of CAA.

The main strength of this study is the diagnostic certainty of our D-CAA study population. As previously mentioned, this allows us to study D-CAA – that can be considered as a monogenetic model for sporadic CAA – over the whole disease course. This also enabled the study of a relatively pure form of vascular reactivity and microstructural white matter integrity, without age related cofounders. That we look at a relatively pure form is demonstrated by the much smaller annual change in PSMD in a healthy population – from the 1000BRAINS study – than the change observed in our D-CAA cohort, and the resulting similar trend in PSMD as a function of age before and after healthy age correction. The fact that PSMD changes in a healthy population

in a much more subtle fashion than in D-CAA subjects, supports the use of normal age correction as performed in this study as opposed to inclusion of age as covariate in the regression models, which would have resulted in an overestimation of the age effect and underestimation of the disease effect in our cohort. A limitation of the healthy control cohort is that those participants were not scanned at the same scanner with the same sequence as our D-CAA study cohort. Previous research has shown that a similar argumentation is true for the BOLD reactivity parameters; since the BOLD response is much more dominantly influenced by disease duration than age effect,<sup>16</sup> the use of age as co-variate would underestimate any disease affect.

Final strengths of this study are the measures used to assess vascular reactivity and microstructural white matter integrity. In this study we used visually stimulated BOLD fMRI to assess the hemodynamic response as an indication of vascular reactivity. In contrast to other methods to assess hemodynamic response – such as the most used BOLD combined with a CO<sub>2</sub> challenge<sup>44</sup> – visually stimulated BOLD fMRI is easily applicable and most importantly non-invasive. The advantage of using PSMD compared to other diffusion MRI measures to assess microstructural white matter integrity is the robustness of this measure to CSF contamination of the diffusion signal and the robustness to variance in diffusion acquisition parameters, MR system, and field strength.<sup>28,45</sup> Robustness to this variance also contributes to our choice to perform healthy age correction to the PSMD data, based on an external cohort.

To conclude, we showed that microstructural white matter integrity is related to a delayed and lowered BOLD response. Importantly, the relationship between PSMD and the lowered BOLD response only starts to appear when the vascular response is severely lowered. These results indicate that there is an interplay between the vascular reactivity deterioration and microstructural white matter integrity loss in D-CAA. Whether this relation is causal cannot be inferred based on these results as the current study is a cross-sectional, observational study.

### Funding

The author(s) disclosed receipt of the following financial support for the research, authorship, and/or publication of this article: HBCx has received funding from the Dutch Heart Foundation under grant agreement 2018-28.

### Declaration of conflicting interests

The author(s) declared the following potential conflicts of interest with respect to the research, authorship, and/or publication of this article: M.R. Schipper reports independent

support from the TRACK D-CAA consortium, consisting of Alnylam, Biogen, the Dutch CAA foundation, Vereniging HCHWA-D, and researchers from Leiden, Boston, and Perth. N. Vlegels reports support by the Dutch Heart Foundation. T.W. van Harten reports no disclosures. I. Rasing reports no disclosures. E.A. Koemans reports no disclosures. S. Voigt reports no disclosures. A. de Luca reports independent support from Alzheimer Nederland (WE-03-2022-11) as well as from ZonMW. K. Kaushik reports no disclosures. E.S. van Etten reports no disclosures. E.W. van Zwet reports no disclosures. G.M. Terwindt reports independent support from the Dutch Research Council (NWO), European Community, the Dutch Heart Foundation, the Dutch Brain Foundation, and the Dutch CAA foundation. G.J. Biessels reports support through the HBC (Heart-Brain Connection) Consortium, funded by the Netherlands CardioVascular Research Initiative, involving the Dutch Heart Foundation (CVON 2018-28 & 2012-06 Heart Brain Connection), Dutch Federation of University Medical Centers, the Netherlands Organization for Health Research and Development, and the Royal Netherlands Academy of Sciences. M.J.P. van Osch reports support by a NWO-VICI grant (016.160.351) and a NWO-Human Measurement Models 2.0 grant (18969) as well as support from the Dutch Research Council (NWO), European Community, the Dutch Heart Foundation, and the Dutch Brain Foundation. M.A.A. van Walderveen reports no disclosures. M.J.H. Wermer reports independent support from the Dutch Research Council (NWO) ZonMw (VIDI grant 91717337), the Netherlands Heart Foundation (Dekker grant 2016T86), and the Dutch CAA foundation.

**Data availability statement**

Data will be shared upon reasonable request after signing a data transfer agreement.

**Authors' contributions**

M.R. Schipper Substantial contributions to conception and design, analysis and interpretation of data. Drafting the article and revising the article critically for important intellectual content. Final approval of the version to be published.

N. Vlegels Substantial contributions to conception and design, analysis and interpretation of data. Drafting the article and revising the article critically for important intellectual content. Final approval of the version to be published.

T.W. van Harten Substantial contributions to acquisition of data, analysis and interpretation of data.

Continued

I. Rasing

E.A. Koemans

S. Voigt

A. de Luca

K. Kaushik

E.S. van Etten

E.W. van Zwet

G.M. Terwindt

G.J. Biessels

M.J.P. van Osch

M.A.A. van Walderveen

Revising the article critically for important intellectual content. Final approval of the version to be published.

Substantial contributions to acquisition of data. Revising the article critically for important intellectual content. Final approval of the version to be published.

Substantial contributions to acquisition of data. Revising the article critically for important intellectual content. Final approval of the version to be published.

Substantial contributions to acquisition of data. Revising the article critically for important intellectual content. Final approval of the version to be published.

Substantial contributions to analysis and interpretation of data. Revising the article critically for important intellectual content. Final approval of the version to be published.

Substantial contributions to acquisition of data. Revising the article critically for important intellectual content. Final approval of the version to be published.

Substantial contributions to conception and design and to analysis and interpretation of data. Revising the article critically for important intellectual content. Final approval of the version to be published.

Substantial contributions to analysis and interpretation of data. Revising the article critically for important intellectual content. Final approval of the version to be published.

Substantial contributions to conception and design and to analysis and interpretation of data. Revising the article critically for important intellectual content. Final approval of the version to be published.

Substantial contributions to conception and design. Revising the article critically for important intellectual content. Final approval of the version to be published.

Substantial contributions to conception and design and to analysis and interpretation of data.. Revising the article critically for important intellectual content. Final approval of the version to be published.

Substantial contributions to conception and design and to analysis and interpretation of data.. Revising the article critically for important intellectual content. Final approval of the version to be published.

(continued)

(continued)

Continued



M.J.H. Wermer Substantial contributions to conception and design and to analysis and interpretation of data. Revising the article critically for important intellectual content. Final approval of the version to be published.

## Acknowledgements

This work is part of the Heart-Brain Connection crossroads (HBCx) consortium of the Dutch CardioVascular Alliance (DCVA).

## ORCID iDs

Manon R Schipper  <https://orcid.org/0000-0003-1463-0997>  
 Thijs W van Harten  <https://orcid.org/0000-0002-3408-9379>

Kanishk Kaushik  <https://orcid.org/0000-0003-1429-6853>  
 Matthias JP van Osch  <https://orcid.org/0000-0001-7034-8959>

## Supplementary material

Supplemental material for this article is available online.

## References

1. Aguilar MI and Brott TG. Update in intracerebral hemorrhage. *Neurohospitalist* 2011; 1: 148–159.
2. Vonsattel JP, Myers RH, Hedley-Whyte ET, et al. Cerebral amyloid angiopathy without and with cerebral hemorrhages: a comparative histological study. *Ann Neurol* 1991; 30: 637–649.
3. Charidimou A, Linn J, Vernooij MW, et al. Cortical superficial siderosis: detection and clinical significance in cerebral amyloid angiopathy and related conditions. *Brain* 2015; 138: 2126–2139.
4. Reijmer YD, van Veluw SJ and Greenberg SM. Ischemic brain injury in cerebral amyloid angiopathy. *J Cereb Blood Flow Metab* 2016; 36: 40–54.
5. Greenberg SM and Charidimou A. Diagnosis of cerebral amyloid angiopathy. *Stroke* 2018; 49: 491–497.
6. Perosa V, Oltmer J, Munting LP, et al. Perivascular space dilation is associated with vascular amyloid-beta accumulation in the overlying cortex. *Acta Neuropathol* 2022; 143: 331–348.
7. Dumas A, Dierksen GA, Gurol ME, et al. Functional magnetic resonance imaging detection of vascular reactivity in cerebral amyloid angiopathy. *Ann Neurol* 2012; 72: 76–81.
8. Peca S, McCreary CR, Donaldson E, et al. Neurovascular decoupling is associated with severity of cerebral amyloid angiopathy. *Neurology* 2013; 81: 1659–1665.
9. Finsterwalder S, Vlegels N, Gesierich B, et al. Small vessel disease more than alzheimer's disease determines diffusion MRI alterations in memory clinic patients. *Alzheimers Dement* 2020; 16: 1504–1514.
10. Salat DH, Smith EE, Tuch DS, et al. White matter alterations in cerebral amyloid angiopathy measured by diffusion tensor imaging. *Stroke* 2006; 37: 1759–1764.
11. Reijmer YD, Fotiadis P, Martinez-Ramirez S, et al. Structural network alterations and neurological dysfunction in cerebral amyloid angiopathy. *Brain* 2015; 138: 179–188.
12. Reijmer YD, Fotiadis P, Charidimou A, et al. Relationship between white matter connectivity loss and cortical thinning in cerebral amyloid angiopathy. *Hum Brain Mapp* 2017; 38: 3723–3731.
13. van Veluw SJ, Reijmer YD, van der Kouwe AJ, et al. Histopathology of diffusion imaging abnormalities in cerebral amyloid angiopathy. *Neurology* 2019; 92: e933–e943.
14. Bakker E, van Broeckhoven C, Haan J, et al. DNA diagnosis for hereditary cerebral hemorrhage with amyloidosis (Dutch type). *Am J Hum Genet* 1991; 49: 518–521.
15. Zhang-Nunes SX, Maat-Schieman ML, van Duinen SG, et al. The cerebral beta-amyloid angiopathies: hereditary and sporadic. *Brain Pathol* 2006; 16: 30–39.
16. van Opstal AM, van Rooden S, van Harten T, et al. Cerebrovascular function in presymptomatic and symptomatic individuals with hereditary cerebral amyloid angiopathy: a case-control study. *Lancet Neurol* 2017; 16: 115–122.
17. Shirzadi Z, Yau WW, Schultz SA, DIAN Investigators, et al. Progressive white matter injury in preclinical dutch cerebral amyloid angiopathy. *Ann Neurol* 2022; 92: 358–363.
18. Woolrich M, Ripley B, Brady M, et al. Temporal autocorrelation in univariate linear modeling of FMRI data. *NeuroImage* 2001; 14: 1370–1386.
19. Jenkinson M, Bannister P, Brady M, et al. Improved optimization for the robust and accurate linear registration and motion correction of brain images. *NeuroImage* 2002; 17: 825–841.
20. Smith SM. Fast robust automated brain extraction. *Hum Brain Mapp* 2002; 17: 143–155.
21. Beckmann CF and Smith SM. Probabilistic independent component analysis for functional magnetic resonance imaging. *IEEE Trans Med Imaging* 2004; 23: 137–152.
22. Amunts K, Malikovic A, Mohlberg H, et al. Brodmann's areas 17 and 18 brought into stereotaxic space-where and how variable? *Neuroimage* 2000; 11: 66–84.
23. Andersson JLR, Jenkinson M and Smith S Non-linear registration, aka Spatial normalisation FMRIB technical report TR07JA2. *FMRIB Analysis Group of the University of Oxford* 2007; 2: e21.
24. Smith SM, Jenkinson M, Woolrich MW, et al. Advances in functional and structural MR image analysis and implementation as FSL. *NeuroImage* 2004; 23 Suppl 1: S208–S219.
25. MathWorks I. *MATLAB: the language of technical computing: computation, visualization, programming: installation guide for UNIX version 5*. Natwick: Math Works Inc., 1996.
26. Tournier JD, Smith R, Raffelt D, et al. MRtrix3: a fast, flexible and open software framework for medical image

- processing and visualisation. *NeuroImage* 2019; 202: 116137.
27. Kellner E, Dhital B, Kiselev VG, et al. Gibbs-ringing artifact removal based on local subvoxel-shifts. *Magn Reson Med* 2016; 76: 1574–1581.
  28. Baykara E, Gesierich B, Adam R, et al. A novel imaging marker for small vessel disease based on skeletonization of white matter tracts and diffusion histograms. *Ann Neurol* 2016; 80: 581–592.
  29. Smith SM, Jenkinson M, Johansen-Berg H, et al. Tract-based spatial statistics: voxelwise analysis of multi-subject diffusion data. *NeuroImage* 2006; 31: 1487–1505.
  30. Charidimou A, Martinez-Ramirez S, Reijmer YD, et al. Total magnetic resonance imaging burden of small vessel disease in cerebral amyloid angiopathy: an imaging-pathologic study of concept validation. *JAMA Neurol* 2016; 73: 994–1001.
  31. Caspers S, Moebus S, Lux S, et al. Studying variability in human brain aging in a population-based german cohort-rationale and design of 1000BRAINS. *Front Aging Neurosci* 2014; 6: 149.
  32. Beaudet G, Tsuchida A, Petit L, et al. Age-related changes of peak width skeletonized mean diffusivity (PSMD) across the adult lifespan: a multi-cohort study. *Front Psychiatry* 2020; 11: 342.
  33. R Development Core Team. *R: a language and environment for statistical computing*. Vienna, Austria: R Foundation for Statistical Computing, 2010.
  34. Johnstone T, Ores Walsh KS, Greischar LL, et al. Motion correction and the use of motion covariates in multiple-subject fMRI analysis. *Hum Brain Mapp* 2006; 27: 779–788.
  35. Koemans EA, Chhatwal JP, Van Veluw SJ, et al. Progression of cerebral amyloid angiopathy: a pathophysiological framework. *Lancet Neurol* 2023; 22: 632–642.
  36. Harris JJ and Attwell D. The energetics of CNS white matter. *J Neurosci* 2012; 32: 356–371.
  37. Masuda J, Tanaka K, Ueda K, et al. Autopsy study of incidence and distribution of cerebral amyloid angiopathy in hisayama, Japan. *Stroke* 1988; 19: 205–210.
  38. Vinters HV and Gilbert JJ. Cerebral amyloid angiopathy: incidence and complications in the aging brain. II. The distribution of amyloid vascular changes. *Stroke* 1983; 14: 924–928.
  39. Smith EE, Vijayappa M, Lima F, et al. Impaired visual evoked flow velocity response in cerebral amyloid angiopathy. *Neurology* 2008; 71: 1424–1430.
  40. Van Dijk SE, Van Der Grond J, Lak J, et al. Longitudinal progression of magnetic resonance imaging markers and cognition in Dutch-type hereditary cerebral amyloid angiopathy. *Stroke* 2022; 53: 2006–2015.
  41. Van Dijk SE, Lak J, Drenth N, et al. Aging effect, reproducibility, and test–retest reliability of a new cerebral amyloid angiopathy MRI severity marker – cerebrovascular reactivity to visual stimulation. *J Magn Reson Imaging* 2023; 57: 909–915.
  42. Van Harten TW, Van Rooden S, Koemans EA, et al. Impact of region of interest definition on visual stimulation-based cerebral vascular reactivity functional MRI with a special focus on applications in cerebral amyloid angiopathy. *NMR Biomed* 2023; 36: e4916.
  43. Switzer AR, McCreary C, Batool S, et al. Longitudinal decrease in blood oxygenation level dependent response in cerebral amyloid angiopathy. *Neuroimage Clin* 2016; 11: 461–467.
  44. Sleight E, Stringer MS, Marshall I, et al. Cerebrovascular reactivity measurement using magnetic resonance imaging: a systematic review. *Front Physiol* 2021; 12: 643468.
  45. McCreary CR, Beaudin AE, Subotic A, et al. Cross-sectional and longitudinal differences in peak skeletonized white matter mean diffusivity in cerebral amyloid angiopathy. *Neuroimage Clin* 2020; 27: 102280.